CHEMISTRY OF MATERIALS
Article

*Chem. Mater.* **2010,** *22,* 117–129 117
DOI:10.1021/cm902469c

# Competing Mechanisms in Atomic Layer Deposition of $Er_2O_3$ versus $La_2O_3$ from Cyclopentadienyl Precursors

Michael Nolan* and Simon D. Elliott

*Tyndall National Institute, University College Cork, Lee Maltings, Prospect Row, Cork, Ireland*

*Received August 12, 2009. Revised Manuscript Received November 12, 2009*

Thin films of rare earth metal oxides are interesting materials for many technology applications, which requires a method for controlled growth of such films. If suitable precursors are available, atomic layer deposition (ALD) is the method of choice for nanoscale thin film deposition. Previous studies have identified promising cyclopentadienyl-containing ($C_5H_5$, Cp) precursors for rare earth oxide ALD, but little is known about the growth reactions. In this paper, we use first principles periodic density functional theory (DFT) computations to study key reactions in ALD growth of $La_2O_3$ and $Er_2O_3$. We start from the hydroxylated (001) surface of the hexagonal phase as a model for each oxide. To predict the most stable adsorbate once the metal precursor pulse is finished, we analyze the interaction of the precursor molecule with the oxide surface, the energetics of successive ligand eliminations and the resulting surface structures. For $La_2O_3$ we find (i) transfer of hydrogen from the surface to a Cp ligand has a barrier of 0.8 eV, (ii) non-ALD desorption of precursor fragments is favored, (iii) the final adsorption fragment is predicted to be $La(Cp)_2$. In contrast, at the $Er_2O_3$ surface, (i) hydrogen transfers spontaneously from the surface to the adsorbing precursor, (ii) reactive adsorption is thermodynamically favored over desorption, and (iii) the final adsorbate is predicted to be Er(Cp). We predict that ligand elimination is significantly more favorable on surfaces of $Er_2O_3$ relative to $La_2O_3$, and so that $Er_2O_3$ ALD is a better process. We rationalize this as due to stronger Er—O bonding, but also due to the restoration of a less distorted surface. These studies provide new insights into the key reactions occurring during ALD of rare earth oxides and new understanding of experimental findings.

## 1. Introduction

The rare earth (RE) metals run from lanthanum (atomic number 57) to lutetium (atomic number 71), and also include yttrium (atomic number 39) and scandium (atomic number 21). The series shows a range of behavior that is determined by the occupation of the 4f shell and the ionic radius.[1] For instance, all rare earths form metal oxides, with the stoichiometry of the most stable oxide being determined by the electronic configuration and ionic radius of the rare earth.[2] These oxides are of great interest in a number of technologies, such as catalysis[3] and optoelectronics.[4] In electronics, their high dielectric constant ($k = 20 - 30$) makes them promising dielectrics for the transistor gate stack,[5] in high value capacitors[6] or as the interpoly dielectric in advanced memory devices. These applications require the deposition of thin films of either the binary rare earth oxide or with the rare earth as a component in a ternary oxide. In particular, memory applications can require conformal deposition in trenches with high aspect ratios and atomic layer deposition (ALD)[7,8] is the method of choice to achieve this.

In simple terms, metal oxide ALD is a chemical deposition process in which precursor gases for the metal and oxygen are introduced separately into the reaction chamber. The metal precursor (an organometallic complex, $ML_n$, where L is a ligand) adsorbs onto the growing film until the surface is saturated with precursor fragments. Any species that are not surface bound are purged from the chamber and the oxygen-containing precursor (e.g., water or ozone) is introduced. Interaction of this species with the surface-bound adsorbate results in formation of —M—O— bonds and submonolayer growth of the oxide. By varying the number of precursor cycles, the thickness of the film can be finely controlled.

A mechanism for oxide film growth has been developed from studies of ALD growth of alumina from

*Corresponding author. E-mail: michael.nolan@tyndall.ie.

(1) Izyumov, Y. A.; Kumarev, E. Z. *Phys.−Usp.* **2008**, *51*, 23.
(2) Petit, L.; Svane, A.; Szotek, Z.; Temmerman, W. M. *Phys. Rev. B* **2005**, *72*, 205118.
(3) Sato, S.; Takahashi, R.; Kobune, M.; Gotoh, H. *Appl. Catal., A* **2009**, *356*, 57.
(4) *Rare Earth Oxide Thin Films: Growth, Characterisation and Applications*, Topics in Appled Physics series; Franciulli, M., Giovanna, S., Eds.; Springer: New York, 2007; p 106.
(5) Jinesh, K. B.; Lamy, Y.; Tois E, E.; Besling, W. F. A. *Appl. Phys. Lett.* **2009**, *94*, 252906.
(6) Tsoutsou, D.; Lamagna, L.; Volkos, S. N.; Molle, A.; Baldovino, S.; Schamm, S.; Coulon, P. E.; Fanciulli, M. *Appl. Phys. Lett.* **2009**, *94*, 053504.
(7) Suntola, T. *Mater. Sci. Rep.* **1989**, *4*, 261.
(8) Leskelä, M.; Ritala, M. *Thin Solid Films* **2002**, *409*, 138.


Published on Web 12/04/2009

trimethylaluminium (TMA, $Al(CH_3)_3$) and water.[9−11] This model has been experimentally verified. When TMA adsorbs at a surface terminated with hydroxyl (OH) groups, a proton from a terminal OH group transfers to a methyl ligand of TMA. A $CH_4$ species forms and is eliminated as gas phase methane. Further proton transfer results in elimination of further methyl ligands as $CH_4$.[9] The introduction of water to the reactor eliminates the last methyl ligands and restores the original —Al—OH surface. This mechanism can be characterized as an *adsorption, proton transfer, ligand elimination* process.

Further understanding of the ALD mechanism for oxides comes from capturing the elimination products upon introduction of the precursors to the reactor,[12,13] with a recent example of the order of ligand elimination from the heteroleptic complex $Zr(Cp)_2(Me)(OMe)$ predicted from modeling and confirmed experimentally.[14,15]

The organometallic chemistry of rare earths is dominated by cyclopentadienyl (Cp, $C_5H_5$) complexes,[16] and they have been used as ALD precursors for rare earth oxides. Alkyl substituted Cp-ligands have been used to improve the volatility of the complex, but should not change the basic surface chemistry. Specific examples include $Gd(Me_3Cp)_3$ (Me, $CH_3$) for growth of $Gd_2O_3$ films,[17] $Pr(Cp)_3$ for $PrO_x$ growth,[18] and $Er(CpMe)_3$ [19] for growth of $Er_2O_3$. A number of La−Cp complexes were tested by Niinistö,[20] but had limited stability and were found not to lead to self-limiting ALD growth, but instead to growth via chemical vapor deposition (CVD). Cp-based complexes have also been developed for ALD growth of other important high-$k$ oxides such as $HfO_2$ and $ZrO_2$.[14,15,21]

One interesting finding that emerges from the literature on $RE(Cp)_3$ precursors for ALD of rare earth oxides is that early rare earths, such as $La_2O_3$[20] and $PrO_x$[18] do not show self-limiting ALD. Instead, decomposition of the precursor takes place, which leads at best to CVD (as evidenced by an ever-increasing growth rate with pulse duration). For $La_2O_3$, grown from the $La(^iPrCp)_3$ precursor, Niinistö[20] has found an increasing growth rare with pulse duration. Using the same precursor in alternating pulses with $H_2O$, Eom et al.[22] also deposit a La-based oxide but are unable to give any evidence for ALD.

With $Gd_2O_3$ grown from $Gd(CpMe)_3$, Kukli et al.[23] found that the growth was self-limiting, but that precursor deposition could not be ruled out; Gd is in the middle of the rare earth series. Finally, Er lies at the end of the rare earth series, and the growth of $Er_2O_3$ from $Er(MeCp)_3$ was found to proceed via self-limiting ALD;[19] a growth rate of $1.5 \pm 0.5$ Å/cycle was found at 250 °C, using the $Er(MeCp)_3$ precursor. Thus, it appears that with Cp-based precursors, growth of early rare earth oxides proceeds via CVD, while the later rare earths may show self-limiting ALD. Explaining this finding is the primary goal of the current work.

To develop an ALD reaction mechanism that rationalizes experimental findings, a combination of experiment and first principles modeling is needed. The modeling can be done in two ways. Gas phase cluster models of the oxide are used and the interaction of the precursor with this cluster model can be investigated, for example, for $Al_2O_3$ growth from TMA[24,25] and $HfO_2$ growth from $HfCl_4$.[26] For Cp-based precursors, there has been recent modeling work on $Y_2O_3$ growth on hydroxylated Si(100) from $Y(Cp)_3$[27] and MgO growth on hydroxylated Si(100) from $Mg(Cp)_2$.[28] This model is quite reasonable and yields important results since the interaction at the surface is rather localized. These studies do provide insights into the overall thermodynamics of growth reactions, but they are not models of the growing surface, nor can they provide reliable information on atomic motions during surface reactions, such as activation energies.

In a similar vein, we have previously developed a gas-phase methodology for assessing the intrinsic reactivity of ALD precursors with different metal−ligand combinations.[29] This simple analysis suggests that the Cp ligand will be moderately reactive (less reactive than alkyl ligands, but more reactive than $\beta$-diketonate ligands). While these gas phase computations are useful for screening potential ligands, they cannot capture the details of the interactions between the precursor and the oxide surface.

The second approach is to use a slab model of the surface, periodic in three dimensions, and study the adsorption of the precursor at the surface. This model has a larger computational burden; It is, however, a more realistic representation of precursor-surface interactions

(9) Elliott, S. D.; Greer, J. C. *J. Mater. Chem.* **2004**, *14*, 3246.
(10) Puurunen, R. L. *J. Appl. Phys.* **2005**, *97*, 121301.
(11) Dilllon, A. C.; Ott, A. W.; Way, D. J.; George, S. M. *Surf. Sci.* **1995**, *322*, 230.
(12) Juppo, M.; Rahtu, A.; Ritala, M.; Leskelä, M. *Langmuir* **2000**, *16*, 4034.
(13) Niinisto, J.; Rahtu, A.; Putkonen, M.; Ritala, M.; Leskela, M.; Niinisto, L. *Langmuir* **2005**, *21*, 7321.
(14) Elam, J. W.; Elliott, S. D.; Faia, M. C.; Zydor, A.; Hupp, J. T.; Pellin, M. J. *Appl. Phys. Lett.* **2007**, *91*, 253123.
(15) Knapas, K.; Ritala, M. *Chem. Mater.* **2008**, *20*, 5698.
(16) Hong, S.; Marks, T. J. *Acc. Chem. Res.* **2004**, *37*, 673.
(17) Niinistö, J.; Petrova, N.; Putkonen, M.; Niinistö, L.; Arstila, K.; Sajavaara, T. *J. Cryst. Growth* **2005**, *285*, 191.
(18) Kukli, K.; Ritala, M.; Pilvi, T.; Sajavaara, T.; Leskela, M.; Jones, A. C.; Aspinall, H. C.; Gilmer, D. C.; Tobin, P. J. *Chem. Mater.* **2004**, *16*, 5162.
(19) Paivasaari, J.; Niinistö, J.; Arstila, K.; Kukli, K.; Putkonen, M.; Niinistö, L. *Chem. Vap. Deposition* **2005**, *11*, 415.
(20) J. Niinistö, PhD Thesis, Helsinki University of Technology, Finland, **2004**
(21) Niinistö, J.; Putkonen, M.; Niinistö, L.; Kukli, K.; Ritala, M.; Leskelä, M. *J. Appl. Phys.* **2004**, *95*, 84.
(22) Eom, D.; No, S. Y.; Hwang, C. S.; Kim, H. J. *J. Electrochem. Soc.* **2007**, *154*, G49.
(23) Kukli, K.; Hatanpaa, T.; Ritala, M.; Leskela, M. *Chem. Vap. Deposition* **2007**, *13*, 546.
(24) Widjaja, Y.; Musgrave, C. B. *Appl. Phys. Lett.* **2002**, *80*, 3304.
(25) Jeloaica, L.; Estève, A.; Djafari Rouhani, M.; Estève, D. *Appl. Phys. Lett.* **2003**, *83*, 542.
(26) Heyman, A.; Musgrave, C. B. *J. Phys. Chem. B* **2004**, *108*, 5718.
(27) Ren, J.; Zhou, G.; Hu, Y.; Zhang, D. W. *Appl. Surf. Sci.* **2009**, *255*, 7136.
(28) Lu, H-L; Ding, S-J; Zhang, D. W. *J. Phys. Chem. A* **2009**, *113*, 8791.
(29) Elliott, S. D. *Surf. Coat. Technol.* **2007**, *201*, 9076.
(30) Elliott, S. D.; Scarel, G.; Wiemer, C.; Fanciulli, M.; Pavia, G. *Chem. Mater.* **2006**, *18*, 3764.

and of reaction barriers in particular. In our work on oxide ALD, we have successfully used this approach for the growth of alumina from TMA and water,[9] as well as $Al_2O_3$ growth from TMA and ozone.[30] In this paper, we generate slab models of $La_2O_3$ and $Er_2O_3$ surfaces, to compare their ALD reactions. These detailed models allow us to assess the usefulness of the more simple gas phase models. Taken together, these models reveal important aspects of the chemistry underlying growth of oxide thin films with ALD.

As we are interested in changes in bonding, we use first principles density functional theory (DFT) for this problem. The computations start from the assumption that the water step has finished, leaving a hydroxylated surface, which is a key aspect of oxide growth.[7−13,27,28] The metal precursor then adsorbs at a hydroxyl terminated surface. In reality, the as-grown material is often amorphous. Simulation of such an amorphous surface is beyond the scope of these simulations and we make a reasonable assumption that local areas of the growing surface share bonding characteristics with a particular crystalline surface. To facilitate comparison, however, we use the same surface model for both oxides: the hexagonal sesquioxide (001) surface.

The layout of the paper is as follows. Section 2 presents our methodological details. Section 3.1 presents a brief description of results on the gas phase precursor molecules. Section 3.2 presents a brief analysis of the rare earth oxide surfaces and adsorption of the precursors at the bare surface. Section 3.3 shows how the hydroxylated surfaces are constructed as models of the surface after the water containing pulse, whereas Section 3.4 includes our main results on precursor adsorption and ALD reactions at these surfaces. Section 3.5 addresses non-ALD reactions. Section 4 is a discussion of the results and their implications for the mechanism of ALD growth and Section 5 presents our conclusions.

## 2. Materials and Methods

We use periodic density functional theory (DFT), in which the valence electron basis is a set of plane waves,[31] with a kinetic energy cutoff of 396 eV. The Perdew−Burke−Ernzerhof (PBE) approximation[32] to the exchange-correlation functional is used and the projector augmented wave (PAW) method[33] is used for the valence−core interaction. There are 11 valence electrons on La and 9 valence electrons on Er, whereas carbon and oxygen have a [He] core and the standard PAW potential is used for hydrogen. The calculations are not spin polarized; a check of the impact of spin polarization for a number of systems shows that it has no effect. For the bulk oxides, $k$-point sampling is performed with a $4 \times 4 \times 4$ Monkhorst−Pack sampling grid. For the surface model of the hexagonal (001) surface, $4 \times 4 \times 1$, $2 \times 2 \times 1$ and Γ-point sampling grids are used for the $(1 \times 1)$, $(2 \times 2)$, and $(3 \times 3)$ surface expansions, respectively. The bulk lattice constants are determined using the Murnaghan equation of state.[34] For surface calculations, the (001) surface is a type II surface,[35] in which trilayers of $RE_2O_3$ stoichiometry are present per $(1 \times 1)$ surface unit cell and we use a slab thickness of four trilayers. The surface energy is computed as

$$E^{\text{surf}} = \{E(\text{slab}) - NE(\text{bulk})\}/2A$$

where $E$(slab) is the total energy of the slab model, $E$(bulk) is the energy of the bulk oxide, $N$ scales the bulk total energy to the same number of atoms as the slab model and $A$ is the area of the surface cell, with the factor 2 accounting for the two faces of the slab. At a slab thickness of four trilayers, the surface energies are converged to 0.01 $Jm^{-2}$.

The largest surface cell expansion uses a thinner slab model with three $RE_2O_3$ trilayers, to reduce the computational burden. Fermi level smearing is performed using the Methfessel−Paxton approach, with the parameter $\sigma$ set to 0.1 eV.[36] A quasi-Newton algorithm is used for ionic relaxation with all ions relaxed (unless otherwise noted) until the forces on the ions are less than 0.02 eV/Å. The molecular geometries of the precursor molecules, $RE(Cp)_3$, $RE(CH_3)_3$, CpH and water are individually relaxed in a box of dimensions $20 \times 20 \times 20$ Å, with a 396 eV cutoff energy and Γ-point sampling.

In constructing the hydroxylated surface, we have to determine physically reasonable hydroxylation coverages. It has been determined that early rare earth oxides, for example, $La_2O_3$ and later rare earth oxides, for example, $Er_2O_3$, react very differently with water.[37] Therefore, a method is needed to separately, but consistently, determine their degree of hydroxylation. The $(1 \times 1)$ surface cell can accommodate one water molecule and on both oxides, water is preferentially adsorbed molecularly, even when starting from a dissociatively adsorbed configuration. The $(3 \times 3)$ surface cell can accommodate nine water molecules and we find that one water molecule (coverage of 1/9) prefers to adsorb dissociatively. Therefore the optimum coverage of surface−OH lies between these extremes.

With this in mind, to obtain an optimum OH coverage, we begin with nine water molecules dissociatively adsorbed on each oxide surface, giving 18 surface−OH groups. DFT molecular dynamics is performed in the NVT ensemble at 500 K for 1 ps. At the end of this process, there is a mixture of molecularly adsorbed water and surface hydroxyl groups. The molecular water is weakly bound at the surface and is removed. The structure is relaxed at 0 K, any further water that forms is removed and the structure relaxed again. The resulting model of a hydroxylated surface is used for subsequent calculations of precursor adsorption.

For these computations, the adsorption energy of the precursor is computed from

$$E^{\text{ads}} = E[\text{precursor−surface}] - [E(\text{precursor}) + E(\text{surface})] \quad (1)$$

where $E$[precursor-surface] is the total DFT energy (at 0 K) of the precursor−surface species, $E$(precursor) is the total DFT energy of the gas phase precursor molecule, and $E$(surface) is the total DFT energy of the hydroxylated surface. To study the stability of adsorbed precursors and surface bound intermediates

(31) Kresse, G.; Furthmüller, J. *Comput. Mater. Sci.* **1996**, *6*, 15; Kresse, G.; Furthmüller, J. *Phys. Rev. B* **1996**, *54*, 11169.
(32) Perdew, J. P.; Burke, K.; Ernzerhof, M. *Phys. Rev. Lett.* **1996**, *77*, 3865.
(33) Blöchl, P. E. *Phys. Rev. B* **1994**, *50*, 17953; Kresse, G.; Joubert, D. *Phys. Rev. B* **1999**, *59*, 1758.
(34) Murnaghan, F. D. *Proc. Natl. Acad. Sci. U.S.A.* **1944**, *30*, 244.
(35) Tasker, P. W. *J. Phys. C* **1979**, *12*, 4977.
(36) Methfessel, M.; Paxton, A. T. *Phys. Rev. B* **1989**, *40*, 3616.
(37) Nagao, M.; Hamano, H.; Hirata, K.; Kumashiro, R.; Kuroda, Y. *Langmuir* **2003**, *91*, 9201.

at temperatures and pressures present during a growth experiment, we estimate contributions to the entropy of the gas phase desorption products, following refs 9,38. The translational entropy of the precursor is given by the Sackur−Tetrode equation

$$\Delta S^{\text{trans}} = S^{\text{trans}}(\text{precursor}) = k \ln\left(\frac{kT}{(p\lambda^3)}\right) + \frac{5}{2}k \qquad (2)$$

where $k$ is the Boltzmann constant, $T$ is the temperature, $p$ is the pressure, $\lambda$ is the thermal wavelength, $\lambda = \sqrt{h^2/2\pi mkT}$, and $m$ is the molecular mass. The rotational entropy of the precursor is approximately given by the expression for a rigid symmetric rotor

$$\Delta S^{\text{rot}} = S^{\text{rot}}(\text{precursor}) = k \ln\left(\frac{1}{\sigma}\left(\frac{kT}{h}\right)^{3/2}\left(\sqrt{\frac{\pi}{B_x^2 B_z}}\right)\right) \qquad (3)$$

where $\sigma$ is the order of the rotational subgroup of the molecular symmetry point group, $B_x$ and $B_z$ are the rotational constants of the molecule perpendicular to and parallel to its symmetry axis, which are related to the moment of inertia, $B_x = \hbar/4\pi I_x$. We use only the precursor entropy since $S^{\text{rot}}$ and $S^{\text{trans}}$ for the oxide surface are approximately zero. The vibrational entropy contribution is neglected since it is approximately constant during the reaction, $\Delta S^{\text{vib}} = 0$. The change in free energy is therefore given by $\Delta G = \Delta E + T\{S^{\text{trans}}(\text{precursor}) + S^{\text{rot}}(\text{precursor})\}$.

Where the hydrogen transfer reaction does not occur in a barrierless fashion, we investigate hydrogen transfer pathways with a constrained optimization procedure to estimate activation barriers. Hydrogen from a surface hydroxyl group is moved along a straight line from surface OH to a carbon atom of the Cp ligand. We have checked a number of means of carrying out the constrained optimization, including constraining the position of hydrogen at each point along this path and allow the remaining ions to relax in response (with the bottom layer of the surface slab fixed) or constraining the hydrogen in a plane, for example in the $(x,y)$ plane. The computed barrier is probably underestimated due to using DFT, as is well-known.[39,40] We are interested in comparing barriers in similar systems, so these systematic errors are approximately constant throughout.

## 3. Results and Discussion

**3.1. Gas Phase Precursors.** Gas phase $RE(Cp)_3$ has a structure in which the ligands have a hapticity of 5, all five carbon atoms in the Cp rings coordinating to the metal. In $La(Cp)_3$, the La—C distances are computed with DFT to be in the range 2.79−2.88 Å, while in $Er(Cp)_3$, the Er—C distances are in the range 2.61−2.72 Å.

For the overall ALD reaction

$$2RE(Cp)_{3(g)} + 3H_2O_{(g)} \rightarrow RE_2O_{3(s)} + 6CpH_{(g)}$$

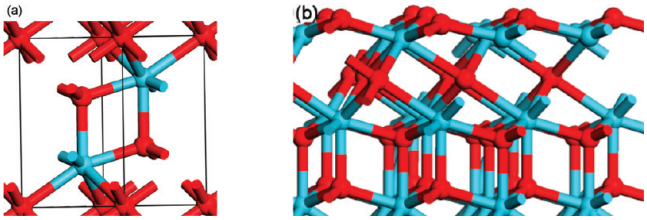


**Figure 1.** Atomic structures of hexagonal $RE_2O_3$. (a) bulk unit cell, (b) side view of (001) surface. The color scheme in this figure is blue for La and red for O, which is used throughout the remainder of the paper.

we compute from first principles that $\Delta E^{\text{ALD}}$ −0.75 eV per $La(Cp)_3$ and $\Delta E^{\text{ALD}} = -1.88$ eV per $Er(Cp)_3$. Thus $Er(Cp)_3$ is more reactive than $La(Cp)_3$ for formation of the oxide by about 1.1 eV per RE atom. As well as bonding changes upon elimination of CpH ligands are eliminated, $\Delta E^{\text{ALD}}$ includes the energy gained upon formation of the bulk oxide.

To consider only the contribution from ligand elimination, we compute the energetics of the following model reaction,[16] denoted $\Delta E^{\text{hyd}}$

$$RE(Cp)_{3(g)} + 3H_2O_{(g)} \rightarrow RE(OH)_{3(g)} + 3CpH(g) \qquad (4)$$

which allows a simple comparison between the reactivity of La and Er precursors with respect to loss of CpH. We find that $\Delta E^{\text{hyd}} = +0.96$ eV of $La(Cp)_3$ and $\Delta E^{\text{hyd}} = +0.42$ eV of $Er(Cp)_3$. Based on this, we therefore expect $Er(Cp)_3$ to be more reactive to ligand elimination by about 0.5 eV per RE atom.

**3.2. Rare Earth Oxide Bulk and Surface and Adsorption at Bare Surfaces.** For bulk $La_2O_3$ and $Er_2O_3$ in the hexagonal structure (space group $P3\overline{m}1$, No. 164), the computed lattice constants are $a$ = 3.9504 Å, $c$ = 6.1538 Å ($La_2O_3$) and $a$ = 3.6705 Å, $c$ = 5.7180 Å ($Er_2O_3$), which are in reasonable agreement with experiment.[41,42] In this structure, Figure 1(a), the metal is 7 coordinated, with three sets of RE—O distances: 2.40, 2.51, and 2.71 Å ($La_2O_3$) and 2.21, 2.29, and 2.55 Å ($Er_2O_3$).

The surface structure for the bare (001) surface is shown in Figure 1(b) and the computed surface energies are 0.44 $Jm^{-2}$ and 0.55 $Jm^{-2}$ for $La_2O_3$ and $Er_2O_3$, respectively. The RE—O distances in the surface layer of the hexagonal (001) surface are 2.37 and 2.37 Å for $La_2O_3$ and 2.05, 2.09, and 2.21 Å for $Er_2O_3$. Surface O—O distances are 3.94 Å ($La_2O_3$) and 3.67 Å ($Er_2O_3$), which are the same as in bulk. Surface cations are 6 coordinate and surface anions are 3 coordinate. Going into the subsurface layer, the distance from surface RE cation to subsurface oxygen is 2.73 Å for $La_2O_3$ and 2.60 Å for $Er_2O_3$, with similar RE—O distances to the next sublayer. Note that Er—O distances are shorter than the corresponding La—O distances.

In Figure 2, we show the structure for the $RE(Cp)_3$ precursor adsorbed at the bare rare earth oxide surfaces,

(38) Atkins, P. W. *Physical Chemistry*, 4th ed.; Oxford University Press: New York, 2004.
(39) Lu, H.-F.; Sun, Y.-C *Surf. Sci.* **2001**, *494*, L787.
(40) Beste, A.; Buchanan, A. C., III; Britt, P. F.; Hathorn, B. C.; Harrison, R. J. *J. Mol. Struct. THEOCHEM* **2008**, *851*, 232.
(41) Wilk, G. D.; Wallace, R. M.; Anthony, J. M. *J. Appl. Phys.* **2001**, *89*, 5243.
(42) Guo, Q.; Zhao, Y.; Jiang, C.; Mao, W. L.; Wang, Z.; Zhang, J.; Wang, Y. *Inorg. Chem.* **2007**, *46*, 6164.

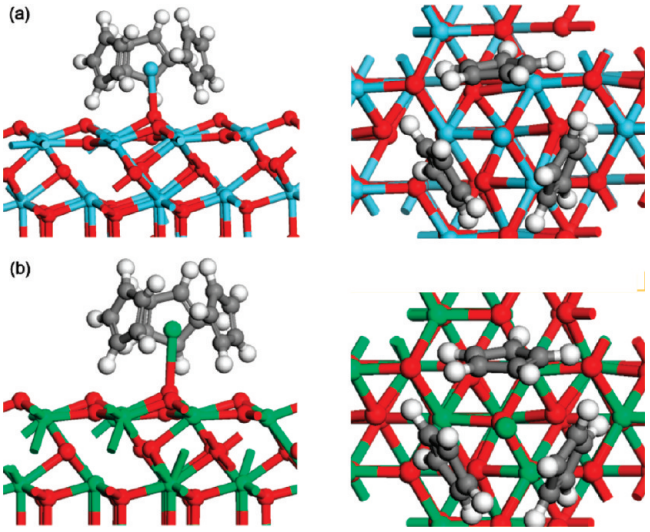


**Figure 2.** Side and plan views of adsorption structures for $RE(Cp)_3$ adsorption at bare (001) surfaces of hexagonal (a) $La_2O_3$ and (b) $Er_2O_3$. For all structures with Er present, the cation is colored green, C is gray, and H is white, and this scheme is used throughout the remainder of the paper.

which we include since it is possible that there are bare areas of oxide surface during growth. For these and subsequent computations, the (3 × 3) surface cell expansion of the (001) surface is used. This expansion gives Cp—Cp distance between periodic images of ca. 7 Å, corresponding to a precursor coverage of 0.83 $La(Cp)_3/nm^2$ and 0.95 $Er(Cp)_3/nm^2$. The adsorption energy is computed from eq 1 and −0.42 eV at $La_2O_3$ and 0.13 eV at $Er_2O_3$.

On both oxides, the energetics of adsorption of the $RE(Cp)_3$ molecule indicate weak or no interactions. For $La_2O_3$, there is a small energy gain for $La(Cp)_3$ adsorption, which is consistent with weak chemisorption at the surface. The La—O distance involving La from the precursor is 2.42 Å, which is consistent with La—O distances in the oxide, and the precursor is little distorted from its gas phase structure. For $Er(Cp)_3$ adsorption at the $Er_2O_3$ surface, the adsorption energy is positive, so that desorption is favored, even without thermal effects. The Er—O distance of 2.73 Å is significantly longer than Er—O distances in the oxide and also indicates no binding of the precursor to the bare surface. The computed adsorption energies indicate that the $La(Cp)_3$ precursor could be weakly bound to the bare oxide, but that the $Er(Cp)_3$ precursor will not be bound at the bare oxide, even at $T = 0$ K.

Looking briefly at the surface structure, we observe that the 3-fold coordinated surface oxygen atom, coordinated to the metal center of the precursor, is pulled out of the surface layer by 0.35 Å for $La_2O_3$ and 0.32 Å for $Er_2O_3$. The displacements of this oxygen on both surfaces are very similar. In addition, the surface oxygen atoms that are nearest neighbors to this oxygen atom, and so lie directly underneath the Cp rings, are displaced downward by 0.80 Å in $La_2O_3$ and 0.50 Å in $Er_2O_3$, and it appears that this reduces the interaction between these surface oxygen atoms and the Cp rings of the precursor, allowing the precursor to come closer to the surface. Such distortion may contribute to the low adsorption energy.

**Table 1. Computed Optimum Hydroxylation Coverage and Adsorption Energy Per Water Molecule on the (001) Surface of Hexagonal $La_2O_3$ and $Er_2O_3$**

| crystal surface | surface area of (3 × 3) surface cell/$nm^2$ | OH coverage/ $OH \cdot nm^{-2}$ | $E^{ads}$/ eV of $H_2O$ |
|---|---|---|---|
| $La_2O_3$ (001) | 1.21 | 5 ± 1 | −0.74 |
| $Er_2O_3$ (001) | 1.05 | 11 ± 1 | −0.25 |

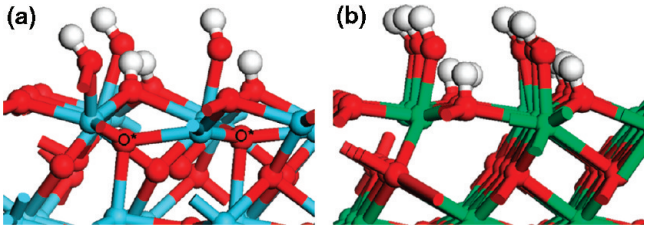


**Figure 3.** Optimum structures for hydroxylation of (001) surfaces (a) $La_2O_3$ and (b) $Er_2O_3$. In (a), the subsurface oxygens indicated as O* were at the surface in the bare oxide (discussed in the text).

We have also examined the $La(Cp)_3$ precursor at the bare oxide surface in a DFT molecular dynamics simulation (300 °C, NVT ensemble, 1 ps run time) and the molecule remains intact and bound in a similar adsorption structure to that in Figure 2. This is in contrast to TMA on $Al_2O_3$, where the molecule undergoes elimination of $CH_3$ in a similar simulation.[9]

**3.3. Adsorption of the $RE(Cp)_3$ Precursor at the Hydroxylated Surfaces.** Before investigating adsorption and reaction of the precursor at the hydroxylated surfaces, we first discuss the model of the surface after the $H_2O$ pulse and purge. The details of the approach we have used are presented in the methods section. The (3 × 3) surface expansion of the (001) surface is used throughout. The coverages and adsorption energies (per water molecule) we have obtained are given in Table 1 and the structures are shown in Figure 3. These hydroxylated surfaces are computed to be energetically the most favorable compared to other coverages (a discussion of hydroxylated surfaces, including temperature and environment effects will be given in a later paper) and are reasonable models of hydroxylated structures resulting from the water pulse and subsequent purge.

On both oxides, the optimum coverage shows a dramatic difference between the oxides, with a significantly higher coverage on $Er_2O_3$ compared to $La_2O_3$. The $Er_2O_3$ surface shows the smaller gain in energy upon hydroxylation (per water molecule and per surface cell) and a larger coverage of surface hydroxyls. These factors could be important for subsequent reactions and we will return to this point in later sections. The substantial energy gain for $La_2O_3$ is consistent with observations that this material is hygroscopic.[42] On both surfaces, the distribution of hydroxyls appears to favor clustering (probably due to interaction between OH dipoles) and the OH groups are found in rows. On the $La_2O_3$ surface, a mixture of

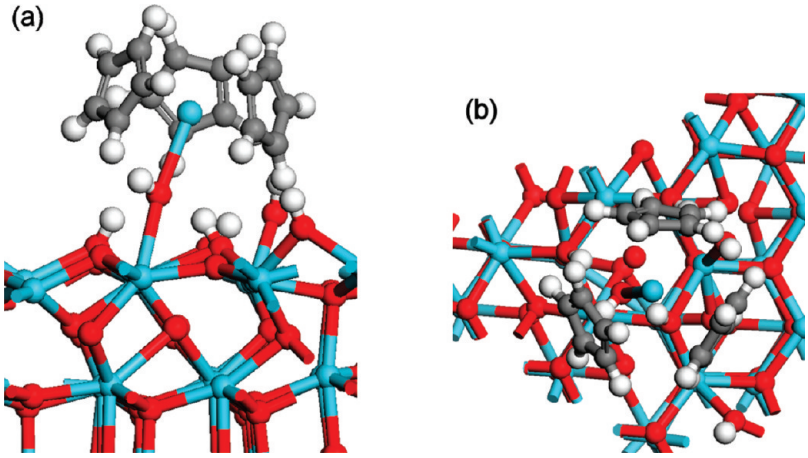


**Figure 4.** Molecular chemisorption of $La(Cp)_3$ at the hydroxylated (001) surface: (a) front view and (b) plan view.

bridging−OH (where oxygen coordinates to two surface cations) and terminal−OH (where oxygen coordinates to a single surface cation) is present, with four bridging−OH groups and 2 terminal−OH groups per (3 × 3) surface cell. On $Er_2O_3$, an equal mixture of terminal−OH and bridging−OH groups are present at the surface. This means that the coverage of terminal−OH groups is over 3 times larger on $Er_2O_3$ than on $La_2O_3$.

Further differences between the oxides arise in their atomic structure. On both surfaces there are distortions around the hydroxyl groups. On the $La_2O_3$ surface, there are quite strong distortions to the surface and the first subsurface layer - in particular, there are two oxygen atoms (indicated as O* in Figure 3(a)) that are repelled from a terminal position into the first subsurface layer. La—O distances involving surface La and nonhydroxyl-terminated surface oxygen are in the range 2.27−2.30 Å, a little shorter compared to the bare surface. La—O distances to oxygen of terminal−OH are 2.35−2.40 Å and to oxygen of bridging−OH are 2.49−2.52 Å. Surface and subsurface La to oxygen distances show a wide spread from 2.39 to 2.66 Å.

On the $Er_2O_3$ (001) surface, strong distortions are evident into the third subsurface layer. In comparison to $La_2O_3$, no surface oxygen atoms move into the subsurface layer. One row of surface Er atoms carrying terminal−OH groups is displaced outward, with the result that the distances from these Er to subsurface oxygen are elongated to 2.67 to 3.06 Å. This distortion appears to be present for both oxides, although where it is found depends on the oxide (subsurface layer for $Er_2O_3$, in the second subsurface layer for $La_2O_3$). This leads to a reduced coordination of cations in both surfaces.

**3.4. ALD Reactions during Rare Earth Precursor Pulse.** In Figure 4 we show the relaxed structure of the $La(Cp)_3$ precursor adsorbed at the hydroxylated (001) surface of the corresponding oxide. As starting structures, the precursor is placed above the OH-terminated surface with the rare earth center initially coordinated to two oxygen atoms and all ions were fully relaxed. A number of other adsorption geometries were tested, but that discussed in this section was the most stable.

The energy gain upon adsorption of $La(Cp)_3$ at the hydroxylated $La_2O_3$ surface is −0.42 eV and the molecule appears to be coordinated to a single oxygen atom of a terminal−OH group. As on the bare surface, this energy change is typical of weak chemisorption. Looking at the atomic structure, the oxygen atom coordinated to the precursor metal center now has a distance of 2.85 Å to a surface La atom (increase of 30%), with a distance of 2.64 Å from this oxygen to the precursor metal center. In the precursor, the La—C distances are consistent with the gas phase molecule, being in the range 2.84−2.92 Å, confirming little distortion to the precursor structure upon adsorption. The distance from the rare earth atom to the center of the Cp rings is 2.54 Å.

Within the surface, changes to La—O distances are generally no more than 0.03 Å compared to the bare hydroxylated surface, indicating only minor distortions upon adsorption of the precursor. The oxygen atoms that sank into the subsurface layer upon hydroxylation remain in this subsurface layer. The elongated La—O distances involving surface La and subsurface La remain (see Section 3.3) after molecular adsorption.

Distances for hydroxyl oxygen to surface La are in the range 2.28−2.46 Å, similar to the bare hydroxylated surface. However, the La—O distance to oxygen of the terminal−OH group coordinated to the precursor is notably longer (see above), indicating that this particular terminal−OH group moves away from the surface to coordinate to the La-center so that the Cp rings are not too close to the surface.

In anticipation of the discussion of ligand elimination in the following section, a key point to note is that no hydrogen is transferred from any of the surface−OH groups to the precursor during the geometry relaxation; we also observed this for other adsorption sites of the precursor, as well as in short DFT molecular dynamics simulations at temperatures up to 300 °C. This indicates a barrier to transfer of hydrogen from the surface to the precursor, which will be elaborated upon later in this section.

On $Er_2O_3$, for which the adsorption structure is shown in Figure,5 the adsorption of the precursor is very

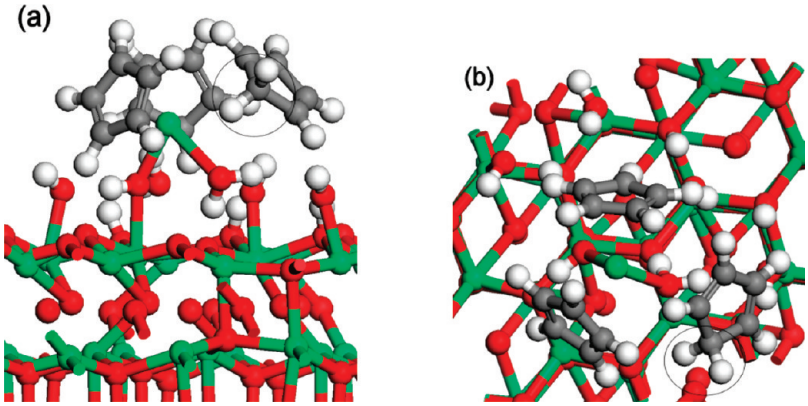


**Figure 5.** Reactive adsorption of $Er(Cp)_3$ at the hydroxylated (001) surface: (a) front view and (b) plan view. The $CH_2$ unit that results from spontaneous hydrogen transfer from the surface to Cp is highlighted within CpH.

different. In this case, we find that during the geometry relaxation, hydrogen transfers from a surface hydroxyl group to one of the Cp rings of the precursor. This finding shows that the hydrogen transfer reaction is barrierless. A CpH moiety is formed, and this is the expected elimination product. We find that individual Er—C distances to this CpH ring are in the range 3.5−4.5 Å (the distance from the rare earth ion to the center of this CpH ring is 3.74 Å), showing that the CpH moves away from the precursor and is lost. Further discussion of ligand elimination will be given later in this section. The distance from the rare earth to the other Cp rings is 2.38 Å.

In forming this species upon adsorption, there is a gain in energy of 3.4 eV, showing a very strong interaction between the precursor and the surface. This is the only surface of these oxides on which we have found find such a large energy gain upon adsorption accompanied by hydrogen transfer to the precursor. The large gain in energy upon adsorption could also be due to the easier formation of CpH (compared to $La(Cp)_3$ at the $La_2O_3$ surface) and the elimination of steric repulsion and associated surface distortion.

Looking at the structure, the precursor metal center is coordinated to two surface hydroxyl groups, with Er—O distances of 2.40 Å; in fact, one of these hydroxyl groups has also accepted a surface hydrogen to become molecular $H_2O$. The distances of these oxygen atoms to surface Er are 2.22/2.24 Å. We therefore find that hydrogen atoms at the hydroxylated surface are rather mobile − one hydrogen is transferred to the precursor and one hydrogen atom migrates to a neighboring OH group to form $H_2O$. This could arise from the high coverage of −OH groups at this surface (Table 1) and the smaller hydroxylation energy at the $Er_2O_3$ (001) surface, particularly when comparing both quantities to the corresponding $La_2O_3$ surface.

In the surface itself, the adsorption and hydrogen migration reactions reduce some of the distortion to the surface that was present upon water adsorption. For example, where previously elongated surface Er to subsurface O distances of 2.54−2.74 Å were present, the same Er—O distances are now 2.26 − 2.35 Å, more consistent with the Er—O distances in the oxide. Similar reductions in other Er—O distances are found and this shows that the reactions taking place during precursor adsorption reduce the distortions to the oxide induced by the introduction of water.

The next step in the adsorption-elimination mechanism is the transfer of a proton from a surface hydroxyl to Cp of the precursor. For $Er_2O_3$, this was found to occur spontaneously, whereas for $La_2O_3$, it was not observed during the geometry relaxation. Thus, for the latter, we investigate what barrier exists for proton transfer. This is done by displacing a proton along a path from the surface to a carbon of a Cp ligand in a constrained optimization procedure, as discussed in Section 2, with the results presented below obtained by fixing hydrogen only in the $z$ direction along the hydrogen transfer path. While somewhat crude this does give a reasonable lower limit on the magnitude of the energy barrier for proton transfer: in the literature, hydrogen transfer barriers computed with DFT are underestimated. However, since we are interested in comparing the barrier between similar systems, systematic errors should be eliminated.

Using this constrained optimization, the barrier for hydrogen transfer from a surface−OH group at the $La_2O_3$ surface to a Cp ligand is estimated to be 0.8 eV. This figure is similar to that computed for the equivalent reaction for TMA at the $Al_2O_3$ surface,[9] indicating that the barrier to proton transfer from OH to a ligand on an oxide surface could generally be of this magnitude. The key structures along the proton transfer path (initial adsorption structure, transition state, and final structure) are shown in Figure 6.[43] In this proton transfer reaction, the proton approaches from behind the ring and as it comes closer to the $sp^2$ CH, the existing hydrogen tilts out of the molecular plane until an $sp^3$ hybridized $CH_2$ is formed. The maximum along this pathway occurs as the proton forms the $sp^3$ hybridized $CH_2$ species; the H—C—H angle is 103°, the C—H distances are 1.12 and 1.10 Å

(43) We have also checked how relaxing the constraints on the proton impacts on the reaction and we find that if the proton is completely free to relax, it will return to the surface, unless it is already bonded to Cp. With the $z$-direction perpendicular to the surface, constraining along $z$ gives results similar to fully constraining the proton, while constraining along $x$ and $y$ gives results similar to having no constraints on the proton.

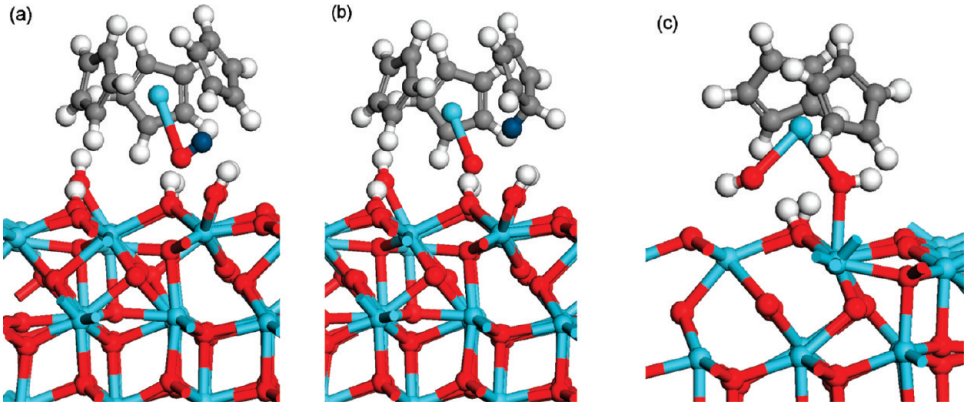


**Figure 6.** Structures for the proton transfer from $La_2O_3$ to the $La(Cp)_3$ precursor determined using the constrained optimization procedure. (a): initial adsorption structure, (b) transition state (structure at the barrier), and (c) $La(Cp)_2$ adsorbate upon proton transfer to a Cp ligand. In parts (a) and (b), the transferred proton is the dark sphere.

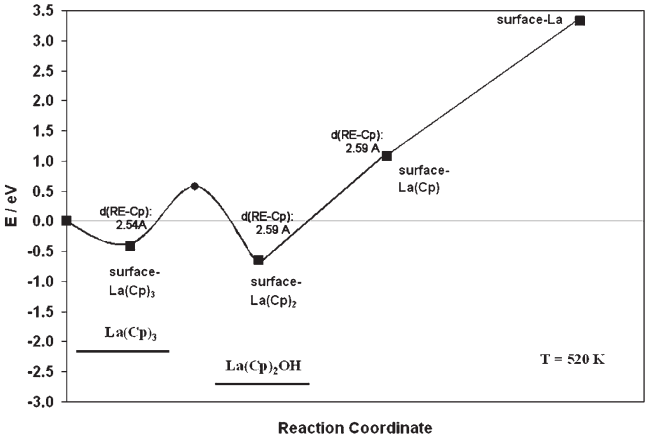


**Figure 7.** Reaction profile for successive elimination of CpH from $La(Cp)_3$ adsorbed at the hydroxylated $La_2O_3$ (001) surface. The zero of energy is separated precursor and hydroxylated surface, the square points mark the relative energies of the structures shown in the figure and the black dot the height of the proton transfer barrier. The horizontal black lines across the bottom of the graph mark the entropy-corrected energies at $T = 520$ K of desorption products $La(Cp)_3$ and $La(Cp)_2OH$ of the $La(Cp)_3$ and $La(Cp)_2$ fragments, respectively. The distance from the rare earth to the center of the Cp ring is also given, as d(RE-Cp) in Å. The thin line joining the points is used to guide the eye.

(to migrating H and H from Cp, respectively) and the O—H distance is 2.05 Å. A minimum is reached upon formation of CpH (with this species moving away from the metal center). Analyzing the electronic structure shows that it is a proton ($H^+$) that is transferred to the Cp ligand.

After adsorption, ligand elimination may proceed by successive hydrogen transfer from the surface to Cp and loss of CpH. When the hydrogen is transferred to Cp of $RE(Cp)_3$, CpH is desorbed leaving $RE(Cp)_2$ at the surface. When a second hydrogen is transferred from the surface to Cp, removal of CpH leaves an RE(Cp) fragment at the surface. For the latter structure our calculations reveal two possible isomers. In the first the Cp ligand remains oriented almost perpendicular to the surface as it is in $RE(Cp)_3$ and the second structure is one in which the Cp ring is rotated to be parallel to the surface. We find that the parallel orientation of the Cp ring is the more stable adsorption structure for both $La_2O_3$ and $Er_2O_3$. Finally, it is conceivable that elimination of the last CpH ligand leaves a bare RE cation at the surface.

To characterize this reaction pathway we show in Figures 7−10 the adsorption structures of the intermediates mentioned above and the reaction profile of the elimination pathway for $La_2O_3$ and $Er_2O_3$, respectively. The reaction profile plots the energy change at $T = 0$ K upon formation of the various intermediate adsorption structures of $RE(Cp)_n$, as well as the barriers for hydrogen transfer, relative to the energy of the initially separated hydroxylated surface and precursor.

For $La_2O_3$, the reaction profile shows that when hydrogen is transferred to Cp and CpH is lost, the reaction of surface adsorbed $La(Cp)_3$ to $La(Cp)_2$ leads to a gain in energy of 0.3 eV. *The $La(Cp)_2$ surface species is thus a potentially stable intermediate* at $T = 0$ K. Transfer of another hydrogen from the surface to $La(Cp)_2$ is uphill and the reaction is so endoergic that the resulting La(Cp) species lies significantly higher in energy than either the separated reactants or adsorbed $La(Cp)_2$. Finally, loss of the last Cp ligand is very unfavorable, with an energy cost of ca. 2 eV. The bare La cation is unstable with respect to readsorption of CpH. Thus the energetics indicate that after introduction of $La(Cp)_3$, transfer of one proton per adsorbate could take place and a single Cp ligand will be eliminated leaving the surface covered with $La(Cp)_2$.

Looking at the structures, in adsorbed $La(Cp)_2$ (Figure 8), the La center is coordinated to two terminal oxygen atoms, with La—O distances of 2.34 and 2.37 Å. These distances are 0.3 Å shorter than the La—O distance in adsorbed $La(Cp)_3$, so that with one less Cp ligand, the adsorbate interacts more strongly with oxygen atoms of the surface, resulting in shorter La—O distances and a gain in energy. The Cp rings have tilted to "open up" the metal center and allow La to move closer to the surface, while maintaining the La—C coordination, with La—C distances in the range 2.83−2.87 Å, slightly shorter than for adsorbed $La(Cp)_3$. This tilting means that steric hindrance arising from the hydrogen atoms of Cp being too close to the surface is avoided.

With LaCp at the surface the most favorable structure has the Cp ring lying parallel to the surface

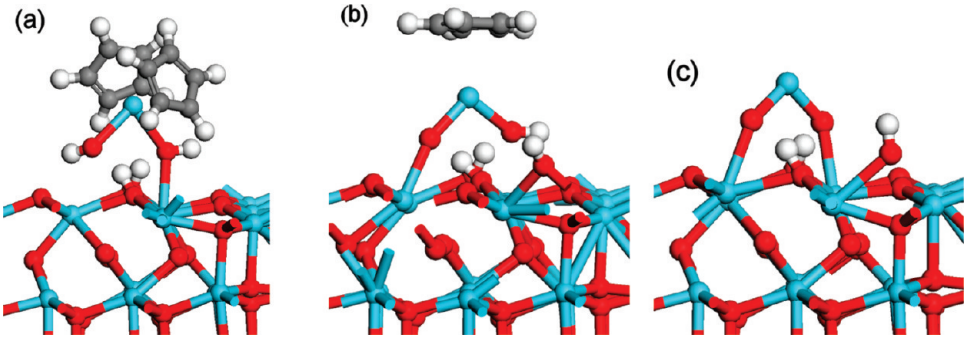


**Figure 8.** Structures in the elimination steps of CpH from the $La(Cp)_3$ precursor at the $La_2O_3$ (001) surface: (a) $La(Cp)_2$ fragment, (b) La(Cp) fragment, and (c) bare La.

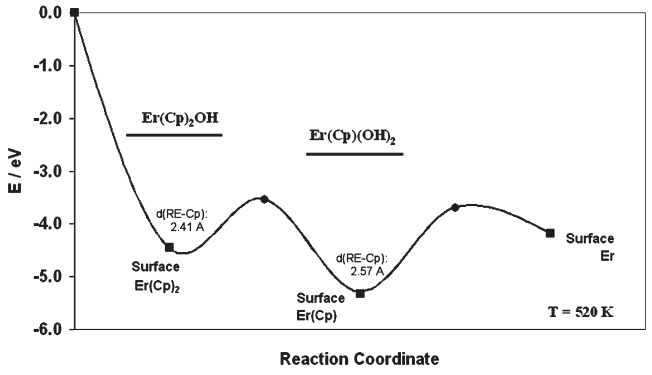


**Figure 9.** Reaction profile for successive elimination of CpH from $Er(Cp)_3$ adsorbed at the hydroxylated $Er_2O_3$ (001) surface. The zero of energy is separated precursor and hydroxylated surface, the square points mark the relative energies of the structures shown in the figure and the black dot the height of the proton transfer barrier. The horizontal black lines across the middle of the graph mark the entropy-corrected energies at $T = 520$ K of the desorption products $Er(Cp)_2OH$ and $Er(Cp)(OH)_2$ of the $Er(Cp)_2$ and Er(Cp) fragments, respectively. The distance from the rare earth to the center of the Cp ring is also given, as d(RE-Cp) in Å. The thin line joining the points is used to guide the eye.

(more favorable by 1 eV over the upright configuration). The metal is still coordinated to two oxygen atoms, with La—O distances of 2.36 Å, little changed from $La(Cp)_2$. However, the La—C distances now lie in the range 2.01−2.43 Å, substantially reduced compared to the gas phase molecule.

Finally, when the last Cp ligand is eliminated, along with a surface H, bare La may be expected at the surface. This La is only two-coordinate, simply because there are not enough oxygens present to have a higher metal coordination. The La ion also protrudes out of the surface, by 1.45 Å relative to the hydroxyl oxygens and has very short La—O distances of 2.00 and 2.02 Å. One might expect that the bare La cation would prefer to sink into the surface in order to coordinate with more oxygen atoms, but instead we observe that La is more stable when it protrudes out of the surface. A possible explanation for this is the ionic radius of the metal compared to the O—O distance between the nearest oxygen atoms coordinated to La. La is a large cation, with an ionic radius of 1.06 Å [44] and the O—O distance in this structure is 3.09 Å, so that La sits above a close packed layer of oxygen and it will be difficult for La to sink toward the surface.

Turning to ligand elimination at $Er_2O_3$, the elimination of CpH giving adsorbed $Er(Cp)_2$, leads to an overall gain in energy of 4.4 eV and Figure 9 shows the reaction pathway for ligand elimination; we show the energy gain for adsorption of $Er(Cp)_3$ and elimination of CpH, since this proceeds in a barrierless fashion. Figure 10 shows the adsorption structures upon elimination of successive CpH ligands. In the $Er(Cp)_2$ adsorption structure, the Er center is two-coordinated to oxygen atoms from surface hydroxyl groups, with Er—O distances of 2.16 and 2.36 Å. The Er—C distances are in the range 2.63−2.68 Å, which are shorter compared to the precursor. On this surface we also observe association of H and OH to form molecular water, which is only seen on the $Er_2O_3$ surface. Again, this arises from a combination of the relatively small energy gain upon hydroxylation and the mobility of hydrogen at this surface, facilitating migration of hydrogen to a neighboring surface OH and formation of water.

The reaction profile in Figure 9 shows that there is a barrier for the transfer of a proton from the surface to a Cp ligand of $Er(Cp)_2$ and the computed barrier from the constrained optimization is ca. 0.8 eV, similar to $La_2O_3$. Once this barrier is surmounted, CpH is eliminated, with a further gain in energy of 1.2 eV and this leaves Er(Cp) bound at the surface. Similar to $La_2O_3$, the Er(Cp) adsorption structure is most stable with the Cp ring parallel to the surface. The metal to carbon distances are in the range 2.65−2.75 Å and the metal center is now 3 coordinate at the surface, with Er—O distances in the range 2.12−2.19 Å, which are similar to surface Er—O distances. The increased coordination of the metal center to surface oxygen stabilizes this adsorption structure and the geometry around the metal center is similar to that of Er in the bare surface, so that Er finds itself in a favorable environment. This is in contrast to La, which is unable to realize such a coordination environment.

Elimination of the final Cp ligand, to leave bare Er at the surface, has a cost of 1 eV, with a proton-transfer barrier of ca. 1.6 eV. The bare Er at the surface is still 3 coordinate, with Er—O distances 2.09−2.15 Å, Er is elevated by 0.16 Å from the terminal oxygen atoms and the reduction in coordination upon loss of CpH presumably

(44) Shannon, R. D.; Prewitt, C. T. *Acta Crystallogr.* **1969**, *B25*, 925; *Acta Crystallogr.* **1970**, *B26*, 1046.

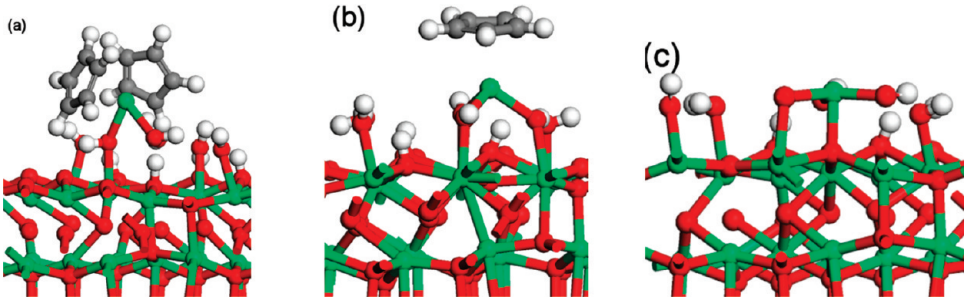


**Figure 10.** Structures in the elimination steps of CpH from the $Er(Cp)_3$ precursor at the $Er_2O_3$ (001) surface: (a) $Er(Cp)_2$ fragment, (b) Er(Cp) fragment, and (c) bare Er.

makes this structure less stable than ErCp. This leads us to conclude that adsorbed Er(Cp) will be the final product during the $Er(Cp)_3$ pulse.

Let us now compare briefly the structures of the bare rare earth cations upon elimination of all ligands from the precursor. For $La_2O_3$, we found that the metal protrudes out of the surface by 1.45 Å and this structure is unstable, but for $Er_2O_3$, the Er atom is contained within the outermost layer of surface atoms (protruding by only 0.16 Å) and is a more favorable structure. On the $La_2O_3$ surface, the O—O distance of the two oxygens coordinated to the cation is 3.09 Å, whereas on $Er_2O_3$, the same O—O distances are 3.57, 3.58, and 3.78 Å. We suggest, that with these longer O—O distances, and loss of all Cp ligands, the smaller $Er^{3+}$ ion (ionic radius 0.89 Å) is better able to migrate into the outermost layer of oxygen atoms, whereas the very large $La^{3+}$ ion (ionic radius 1.06 Å) cannot do so. In addition, the initial hydroxyl coverage may play a role, since the low coverage on $La_2O_3$ leaves fewer terminal oxygen atoms for the metal center of the precursor to react with, whereas for $Er_2O_3$, the high initial coverage provides a larger number of low coordinated oxygen sites.

**3.5. Non-ALD Reactions of the Rare Earth Precursors.** While our results above indicate that $La(Cp)_2$ will be the thermodynamically favored surface bound species after the introduction of $La(Cp)_3$ and a mixture of $Er(Cp)_2$ and Er(Cp) after introduction of $Er(Cp)_3$, we need to consider the possibility of competition between adsorption at the surface and desorption. Desorption can result in decomposition of the precursor above the surface and non-ALD growth. If the entropy cost, $T\Delta S$, of the desorption products of the surface bound intermediate (at a given temperature and pressure) is larger than the adsorption energy, then desorption of the intermediate is favored. This can influence the residence time of the adsorbate at the surface and whether it can undergo further reaction during growth. Using computed gas phase data for possible desorption products, we can compute the compound-specific quantities needed for the translational and rotational entropy in eqs 2 and 3. Due to the large mass of the $La(Cp)_3$ molecule, the translational entropy contributes 1.5 eV to the gas phase free energy, while the rotational contribution is 0.63 eV, under typical ALD conditions,[45] of a pressure of 3 Pa and a temperature of 520 K. Since some vibrational modes will be hardened upon adsorption (e.g., La—O) and others will be softened (e.g., La—C), the vibrational contribution will be small. The sum of the translational and rotational entropy contributions, which is $T\Delta S = 2.13$ eV, should be an upper limit to the entropy change upon adsorption/desorption. Since an adsorbate will desorb if $T\Delta S > -E_{ads}$ and $E_{ads}$ of $La(Cp)_3$ is $-0.42$ eV, we find that desorption of the precursor will be thermodynamically favored (assuming that thermodynamic equilibrium is reached before other reactions occur).

Looking now at the intermediate adsorbates, $La(Cp)_2$ can desorb as neutral $La(Cp)_2OH$, for which $T\Delta S$ is computed to be 2.75 eV. The adsorption energy of $La(Cp)_2OH$ is $-1.62$ eV, which is smaller than the entropic cost and this intermediate should also be subject to desorption. Desorbed $La(Cp)_2OH$ could react with gas-phase $La(Cp)_3$ in a CVD-like reaction, leading to uncontrolled film growth. There is no need to consider the entropy contributions for the other possible $La(Cp)_n$ intermediate structures, since these are computed to be higher in energy than the bare surface and precursor even at $T = 0$ K.

For $Er(Cp)_3$, the total entropy contribution to the free energy is $T\Delta S = 2.15$ eV (1.51 eV for translational and 0.64 eV for rotational contributions, at $p = 3$ Pa and $T = 520$ K), while for the desorption product of surface bound $Er(Cp)_2$, that is $Er(Cp)_2OH$, $T\Delta S = 2.77$ eV. However, the much larger adsorption energy of the various $Er(Cp)_n$ fragments compared to the entropy, allows us to predict that reactive adsorption is favored over thermal desorption. This means that a mixture of surface-bound $Er(Cp)_2$ and Er(Cp) intermediates will be present at the surface for sufficient time to react and facilitate oxide growth, and will be present after the end of a saturating Er precursor pulse.

## 4. Discussion

The results of this paper demonstrate striking differences between surface reactions of Cp-based precursors on $La_2O_3$ and $Er_2O_3$ surfaces, which we now discuss.

A first difference is in the hydroxylation coverage on both (001) surfaces obtained by the method described in Section 2, Section 3.3, and Table 1. The coverage is significantly higher on the $Er_2O_3$ surface, over double

(45) Gallagher, B. K.; Brown, M. E.; Kemp, R. B. *Handbook of Thermal Analysis and Calorimetry*; Elsevier: New York, 2003.

that of the $La_2O_3$ surface, implying that the Er—OH surface is much more Brønsted acidic. At the same time, the gain in energy per adsorbed water is much larger for $La_2O_3$ than for $Er_2O_3$. It is worth keeping these differences in mind in the discussions below.

**4.1. Adsorption.** We find that adsorption of the precursor at the bare surfaces is due to an interaction of the hindered metal center with a surface oxygen atom. However, the adsorption energy for $La_2O_3$ indicates weak molecular chemisorption, probably due to steric repulsion between the precursor and the oxide surface. On bare $Er_2O_3$, there is essentially no chemisorption. This shows that, for both rare earths, bulky Cp ligands make the organometallic precursor quite a weak Lewis acid.

Since in both cases, a terminal oxygen moves out of the surface layer, we can qualitatively investigate the Lewis basicity of the surface by considering the formation energies of a neutral oxygen vacancy at each surface. We make this comparison to investigate how hard it is to pull oxygen out of the surface layer, which is what happens in precursor adsorption and vacancy formation. At the $La_2O_3$ surface, the formation energy of a neutral oxygen vacancy is 6.57 eV (631 kJ/mol), while at the $Er_2O_3$ surface the formation energy is 7.74 eV (743 kJ/mol). Thus on $Er_2O_3$, it will be more difficult to pull oxygen out of the surface to interact with the precursor. We suggest that pulling oxygen out of the surface is needed to prevent the bulky Cp ligands being repelled by the surface.

On the hydroxylated surfaces, the interaction is different for each oxide. On $La_2O_3$, there is a similar gain in energy upon adsorption to that at the bare oxide surface, again indicating weak molecular chemisorption. There is an interaction between terminal oxygen (this time from an OH group) and the metal center of the precursor, as evidenced by the La—O distance and the distortion of this oxygen away from the surface. The long La—O distances keep the ligands from interacting with the OH groups of the surface. Upon adsorption, there is no spontaneous transfer of a proton from any of the surface−OH groups to the precursor. However, the bonding changes on chemisorption are so weak that they can not compete with the entropic cost, under typical ALD conditions, and we conclude that the residence time of $LaCp_3$ at the surface is very low.

On the hexagonal hydroxylated $Er_2O_3$ (001) surface the behavior of $ErCp_3$ is rather different. First, adsorption results in spontaneous proton transfer to the precursor and loss of CpH, yielding a large energy gain (4.4 eV (422 kJ/mol)). We can characterize this interaction as strong reactive chemisorption. Further reasons for the large energy gain upon adsorption of $Er(Cp)_3$ include the coordination of Er from the precursor to multiple terminal hydroxyl oxygens ($La(Cp)_3$ coordinates to only one such oxygen), the favorability of CpH formation and the consequent relief of steric repulsion.

There is thus an array of different adsorption modes, which depend on the atomic-scale structure of the surface and on the intrinsic reactivity of the oxide being grown.

**4.2. Elimination.** As discussed above, the elimination of the first Cp ligand from $Er(Cp)_3$ takes place spontaneously on the $Er_2O_3$ (001) surface, which leads to an adsorbed $Er(Cp)_2$ species and an overall energy gain of 4.4 eV (422 kJ/mol). On the $La_2O_3$ (001) surface, the loss of Cp and formation of an $La(Cp)_2$ species at the surface gives an energy gain of just 0.2 eV (19 kJ/mol), in stark contrast to the energetics for $Er(Cp)_3$. The surface bound $RE(Cp)_2$ species are closer to the surface than the sterically hindered initial precursor, presumably since the loss of one ring opens up the metal center.

The computed energetics for the transformation from $RE(Cp)_2$ to RE(Cp) again highlights the differences between the two rare earths. For $Er_2O_3$, loss of CpH gives a further gain of 1 eV (96 kJ/mol), while for $La_2O_3$ on the other hand, the path for proton transfer is uphill and the energy cost to form LaCp is 1.6 eV (154 kJ/mol). On both surfaces, the loss of the final Cp ligand has an energy cost. However, even here $Er_2O_3$ is more reactive than $La_2O_3$, with only a small energy cost to form the bare $Er^{3+}$ cation at the surface. In these final structures, we observe Er sinking toward the surface and becoming three coordinate, with a structure similar to that in the oxide. In contrast, $La_2O_3$ is unreactive to forming the bare cation and in this structure, the La cation protrudes out of the surface, with a structure distinct from that in the oxide. This gives an indication of the potential gain in energy if bulk-like units of oxide can be formed during ALD.

If we look at the energetics of the gas phase model reaction in eq 4, we see that even in this simple model, $Er(Cp)_3$ is 0.5 eV (48 kJ/mol) more reactive to Cp elimination than $La(Cp)_3$ - suggesting that our present findings are partly intrinsic to the precursor itself. This can arise from the smaller Er cation leading to more crowding of Cp rings. This also contributes to the greater reaction energy for Er in the entire ALD cycle ($\Delta E^{ALD}$ for Er exceeds that for La by 1.1 eV (196 kJ/mol), Section 3.1). A similar trend is seen in experimental enthalpies of formation of the oxides from their elements −18.6 eV (1786 kJ/mol) for $La_2O_3$[46] and −19.7 eV (1891 kJ/mol) for $Er_2O_3$.[46] In addition, the shorter Er—O distances show stronger binding of Er to O than La to O. Thus, there will be a greater driving force for ligand elimination and formation of bonds to O in $Er(Cp)_3$ than in $La(Cp)_3$. However the estimated magnitude of this difference (~1 eV (96 kJ/mol) for Er vs La) is not enough to explain the computed differences in energetics of individual ALD reaction steps.

The key factor appears to be the comparison of hydroxylated $La_2O_3$ and $Er_2O_3$. The latter has a much higher coverage of OH at the surface, particularly terminal−OH, and its lower hydroxylation energy shows that these protons are more thermodynamically reactive. Whether the Er—OH protons are also more kinetically mobile is

(46) Thermochemical Data of Pure Substances, 3rd ed.; Barin, I., VCH: New York, 1995; Vol. *1*.
(47) Olivier, S.; Ducere, J. M.; Mastail, C.; Landa, G.; Estève, A.; Djafari Rouhani, M. *Chem. Mater.* **2008**, *20*, 1555.

discussed below. In addition, adsorption at the $Er_2O_3$ surface also lifts the surface distortions that were initially present at the hydroxylated surface. Such reorganizations of thin film structure in the surface and subsurface layers may make large contributions to energetics along the reaction pathway, but cancel out in global considerations (like $\Delta E^{ALD}$, Section 3.1). The importance of structural reorganization (or "densification") in ALD has been determined from kinetic Monte Carlo simulations.[47]

During some reaction steps, we observe that the energy changes associated with surface reorganization are enough to overwhelm barriers to proton transfer and CpH elimination (Figures 7 and 9). In other cases, we are able to find approximate transition states. Proton transfer and formation of $sp^3$ hybridized $CH_2$ carbon is found to be almost complete at the transition state, and beyond this energy is gained as the CpH moiety moves away and allows the metal to coordinate more closely to the surface. The activation energy is computed to be 0.8 eV (77 kJ/mol) for $La(Cp)_3 \rightarrow La(Cp)_2$ and 0.8 eV (77 kJ/mol) for $Er(Cp)_2 \rightarrow Er(Cp)$, which shows that the RE metal has little influence on the kinetics of proton transfer from OH to Cp.

**4.3. Desorption.** On $La_2O_3$, the estimated entropy contribution to the free energy of the precursor is such that there will be competition between adsorption and desorption, with the energetics favoring desorption of the precursor and intermediates. This means that it is possible that the precursor fragments will not be resident at the surface for sufficient time to undergo ALD reactions. Surface-mediated precursor decomposition, e.g., yielding $La(Cp)_2OH$ from adsorbed $La(Cp)_2$, could lead to an MOCVD process that will not show self-limiting growth. In addition, the inertness of La—OH could lead to the growth of a La hydroxide film. These features that emerge from our simulation of $La_2O_3$ (desorption, decomposition, hydrous film) are possible reasons for the problems faced in experiment when trying to develop the ALD of $La_2O_3$.[20]

By contrast, on $Er_2O_3$ the much greater stability of the surface intermediates means that they are less likely to thermally desorb and so will be available for further reaction, be it proton transfer or the introduction of the oxygen-containing species. Again, this agrees with the successful experimental ALD of $Er_2O_3$.[19]

**4.4. Alternative Oxygen Precursors.** In Section 3.3 we generated surfaces that are saturated with hydroxyl groups, as may be expected to occur at the end of a $H_2O$ precursor pulse in rare earth oxide ALD. Alternatives to $H_2O$ such as $O_2$-plasma or $O_3$ are often used as oxygen sources, and so we discuss here the extent to which the mechanism that we have computed is applicable in these cases.

It is now well-established that surface hydroxyl is present in ALD after an oxidizing precursor strips organic ligands off the growing oxide surface. For instance, hydroxyl has been detected at the end of the oxygen ALD pulse in thermal TMA+$O_3$[30] and TMA+$O_2$-plasma.[48] Indeed, the computed mechanism for the first of these processes reveals one surface−OH being produced for every ligand that is oxidized.[30] Compared to $H_2O$-based ALD, the resulting OH coverage is lower, which as we have seen above, can have a dramatic effect on ALD reactions. Nevertheless, the metal pulse can be expected to proceed in a similar fashion as in the $H_2O$ case, namely via adsorption, proton transfer and ligand elimination. The mechanistic insights obtained here for the metal pulse of $RE(Cp)_3+H_2O$ are therefore directly applicable to the metal pulse of $RE(Cp)_3+O_3$ or $RE(Cp)_3+O_2$-plasma as well.

In the $H_2O$ process, we predict elimination of about 66% of the ligands as HCp during the $Er(Cp)_3$ pulse (Section 3.4). By contrast, because of the self-stabilizing nature of the $O_3$ process,[30] 50% of the HCp should be lost during the Er-pulse in the $O_3$ case. More ligands left on the surface means less adsorption of Er-precursor, and so the growth rate will be correspondingly lower in the $O_3$ process than in the $H_2O$ one. Specifically, dividing 66% by 50%, we predict that the molar growth rate[49] should be about 1.3 times higher with $H_2O$ than with $O_3$.

**4.5. Energy Profiles.** In summary, the general form of the reaction profiles shown in Figures 7 and 9 is endoergic for $La_2O_3$ and exoergic for $Er_2O_3$. This shows that $Er(Cp)_3$ on $Er_2O_3$ is more reactive than $La(Cp)_3$ on $La_2O_3$, with different growth scenarios for each oxide. Let us compare with a validated reaction profile, that of TMA at $Al_2O_3$.[9] In this process, the reaction profile is very similar to $Er_2O_3$, being exoergic. However, we must be cautious with this comparison as it is between different oxides with different precursor ligands.

To look at this point, we investigated hypothetical $RE(CH_3)_3$ precursors at both rare earth oxide surfaces. Figure 11 shows the reaction profiles for $La(CH)_3$ adsorption and $CH_4$ elimination on $La_2O_3$; a similar picture is found for $Er_2O_3$. Here we see that the reaction profile is exoergic up to formation of the bare RE cation, very similar to TMA at $Al_2O_3$.

Thus, the Me-based precursor shows the same factors affecting ALD as in the case of Cp-based precursors. The Lewis acidity of the metal precursor is affected by the size of its ligands ($CH_3$ is much smaller than Cp) and this in turn dictates adsorption energetics. The reactivity of the precursor with respect to ligand elimination contributes to the energetics of further ALD reactions on the surface ($CH_3$ is more reactive than Cp with surface protons). Finally, the Brønsted acidity of the growing oxide also plays a large role, as do reorganizations of the film structure.

Beyond the details of the precursor, the state of the growing surface is a key factor. Uniquely up to now, the present work considers the same set of ALD reactions on

(48) Langereis, E.; Keijmel, J.; van den Sanden, M. C. M.; Kessels, W. M. M. *Appl. Phys. Lett.* **2008**, *92*, 231904.

(49) The thickness increment per cycle depends on the molar increment per cycle and on the density of the film.

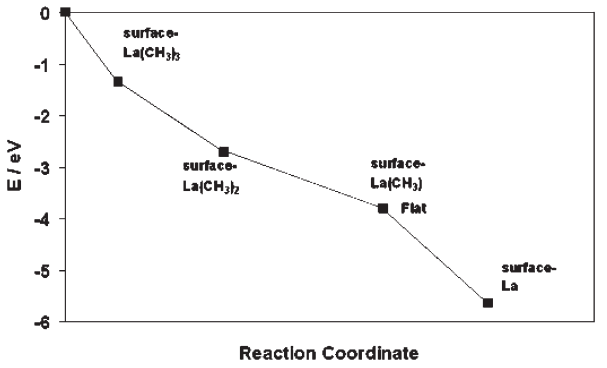


**Figure 11.** Reaction profile for successive elimination of $CH_4$ from La-$(CH_3)_3$ adsorbed at the hydroxylated $La_2O_3$ (001) surface. The zero of energy is separated precursor and hydroxylated surface, the square points mark the relative energies of the structures shown in the figure and the thin line joining the points is used to guide the eye. No reaction barriers were computed.

two metal oxides side by side, and these results shed new light on the importance of the state of the oxide surface during growth. The two rare earth oxide surfaces considered here show dramatically different OH coverages, with that on $Er_2O_3$ being notably larger. In addition, the OH groups at this surface are less stable compared to the $La_2O_3$ surface. These factors combine to make protons more plentiful and more reactive. Thus the transfer of protons to the Cp ligand is more favorable on the $Er_2O_3$ surface and the Cp elimination can continue further in the $RE(Cp)_3$ pulse than on $La_2O_3$. Such ligand elimination is the crucial reaction in ALD. In fact we also see protons diffusing to combine with surface−OH groups to form molecular water during the simulations at the $Er_2O_3$ surface, which we do not see at the $La_2O_3$ surface.

## Conclusions

We have carried out DFT calculations on slab models of the (001) surface of hexagonal $La_2O_3$ and $Er_2O_3$ to investigate the reactions that may occur during ALD of these oxides. Quantitative structures and energetics along the reaction pathway have been obtained, and these have been interpreted with the aid of simpler qualitative models. Alternative non-ALD reactions have also been considered, and we have found evidence that these predominate in the $La_2O_3$ case, in agreement with experiment.

We focus on Cp-based precursors and find that $RE(Cp)_3$ is a hindered Lewis acid that can be unreactive and adsorb weakly. The situation changes when the substrate provides a large number of reactive OH groups, which of course will be determined by the nature of the oxide and the morphology of the surface available. The growing surface that provides the highest coverage of reactive OH groups should be favored during the growth process, and this will ultimately influence the phase of the film that is grown. While the overall energy released in Cp-based ALD is quite modest, substantial reorganizations of the surface atoms can require at least as much energy again, as protons are transferred, bulky ligands are accommodated and new metal−oxygen linkages are formed.

It is clear from our simulations that Cp-based precursors are best suited for growing rare earth oxides where the cation is from the right-hand side of the rare earth row, that is, the smaller rare earths (e.g., $Er_2O_3$). The major reason for this appears to be the higher Brønsted acidity of the hydroxides of the smaller rare earths. A smaller additional factor is the greater intrinsic reactivity of small metals in Cp complexes. Hindered adsorption and lack of available surface protons makes growth of oxides of early rare earths (e.g., $La_2O_3$) difficult using ALD, while the opposite should be true for later rare earths. This explains the range of results obtained when attempting ALD of rare earth oxides.[16−31]

**Acknowledgment.** We acknowledge support from the European Commission through the 6th Framework project "REALISE" (REALISE, NMP4-CT-2006-016172). We acknowledge a grant of computer time at Tyndall from Science Foundation Ireland, and the SFI/Higher Education Authority funded Irish Centre for High End Computing (ICHEC) for the provision of computational facilities.